ON PREDICTION OF WIND-BORNE PLUMES WITH SIMPLE MODELS OF TURBULENT TRANSPORT

KATHERINE SCHWARZ, TAD PATZEK, AND DMITRIY SILIN

Abstract. Two approaches to prediction of wind-borne plumes from sources on the ground are compared: (1) an exact solution to the advection-dispersion equation in steady state, assuming a power-law wind velocity profile; and (2) a numerical simulation of the coupled air-ground system using a logarithmic wind velocity profile. The power-law velocity profile produces less vertical diffusivity and less upward transport compared to the logarithmic velocity profile.If the goal is to predict concentration in the air, the reverse seepage from air to ground is small enough to ignore and the air and ground can be treated as decoupled.

1. Introduction

Predicting the dispersion of air pollutants from sources on the ground requires modeling of turbulent transport. Although a full description of turbulence is beyond either theory or simulation, approximate results can be derived from an analytical model that is relatively simple, while still accounting for the variation with height of wind speed and diffusivity.

Even in the simplified model discussed in this report, few analytical solutions are known. Many well-established models used for regulatory purposes use Gaussian plumes, which are computationally simple, but assume that wind speed and diffusivity are uniform (New Zealand Ministry for the Environment, 2004). As a result, the plume height and decrease of ground-level concentration are underestimated. If the wind speed and diffusivity profiles are assumed to follow power laws, there is a more general analytical solution which is just as easy to compute and potentially more accurate.

This report compares two approaches to modeling leakage of a gas from an underground reservoir into the surface layer of the atmosphere:

(1) Using a known source distribution at the surface as a boundary condition on the differential equation describing admixture transport (Barenblatt, 2003b); and
(2) Simulating both air and ground transport together in a finite-volume code, with a logarithmic wind velocity profile (Oldenburg & Unger, 2004).

The analytical solution applies to a simplified model that assumes an infinite, uniform, flat plane, no change of wind conditions with time, and wind velocity profile in the form of a power law. More realistic descriptions would

require numerical simulation and better modeling of the underlying physics. The approaches discussed here do not actually model turbulence, but rather assume a certain mixing due to turbulence. The purpose of comparing the analytical solution with the coupled simulation is in particular to investigate

- How sensitive is the solution to the velocity profile, and to the exponent in the power law?
- How is the simulation affected by a closed-top boundary condition imposed in the numerical model?

This report first describes the simplest possible model of turbulent diffusion, then compares the two approaches.

2. A simple theoretical picture of turbulent diffusion

Dilute gases, smoke, or dust are usually passive additives to the air: i.e., they do not affect the already existing flow field. If the admixture does not have a density much different from the fluid, settling due to gravity can be neglected. The concentration of a passive additive is governed by the advection-dispersion equation,

$$\partial_t c + \boldsymbol{\nabla} \cdot (\mathbf{u} c) = -\boldsymbol{\nabla} \cdot \mathbf{F} \tag{2.1}$$

where $c(\mathbf{r}, t)$ is the concentration field, $\mathbf{u}(\mathbf{r}, t)$ is wind velocity, and $\mathbf{F}(\mathbf{r}, t)$ is the diffusive flux of the additive due to turbulent mixing. Emission of the additive from a source can be represented by a boundary condition or source term.

All these variables represent averages over rapid turbulent fluctuations. Theoretically the average should be an ensemble average, based on repeating the experiment. But since replicating the same weather conditions is not feasible, ergodicity is assumed so that time averages can be used instead, over intervals of typically 10 minutes to 1 hour (Monin & Yaglom, 1971, sec. 3).

The following sections will discuss the forms of wind velocity and diffusive flux that will be used in equation (2.1).

2.1. Velocity profile in the surface layer.

For sources on the ground, we are concerned with the surface layer of the atmosphere, which is defined as the layer next to the ground where there are strong vertical gradients of velocity, temperature, and concentration. It is typically 10–100 meters thick. In this layer the flow is dominated by surface friction and temperature gradient, and the Coriolis force can be neglected. Wind speed and turbulent mixing vary with height in this layer. We would like to describe the wind velocity profile, $u(z)$, and the turbulent mixing with as few measurable parameters as possible, using similarity theories to group variables into the minimum necessary number of dimensionless parameters. We will need to assume:

- The ground is flat and homogeneous over an area so large that edge effects can be ignored, and therefore the flow field does not depend on the horizontal coordinates, but only on height.

- The air is incompressible ($\boldsymbol{\nabla} \cdot \mathbf{u} = 0$), a good approximation in the surface layer. Together with the first assumption, this then implies that the average vertical component of wind is zero.
- In the conventional coordinate system, z is height above ground and the x axis is chosen along the direction of the average wind. Thus the wind velocity has only an x component, $u(z)$.

Turbulence generated by surface friction. To describe turbulent flow near a surface when there is no heat flux, von Kármán's "law of the wall" is widely used (Arya, 1999, section 4.7.1; Panofsky & Dutton, 1984, section 6.2):

$$\frac{u(z)}{u_*} = \frac{1}{\kappa} \ln \frac{z}{z_0} \tag{2.2}$$

where

- u_* is called the friction velocity, and is defined from the shear stress at the surface, τ, and the air density, ρ, by $u_* = \sqrt{\tau/\rho}$. This shear results from the turbulent fluctuations of velocity:

  $$\tau = -\rho\overline{u'w'}; \text{ so } u_* = \sqrt{-\overline{u'w'}}$$

  where u' and w' are the fluctuating components of horizontal and vertical velocity. Through this covariance a net downward flux of momentum is delivered from the wind to the ground. From this definition it can be seen that u_* is of the same order of magnitude as the fluctuations of velocity.
- κ is von Kármán's constant, which has a value of about 0.4.
- z_0 is a constant of integration, defined as the height at which $u(z) = 0$ when the profile is extrapolated downward (the equation is only valid for $z \gg z_0$). It is called the roughness length, and can be interpreted as the size of eddies at the surface, where momentum is transferred not by skin drag but by form drag across the small irregularities of the surface. The length z_0 is smaller than the actual height of the irregularities, and of course depends on their shape and distribution.

The parameters u_* and z_0 can be determined by measuring $u(z)$ at different heights and fitting a straight line to u vs. $\ln z$.[1] The length z_0 is a characteristic of the surface (unless the surface itself changes, as when grass bends in a high wind), so after z_0 is determined at a particular site, u_* can be found in other wind conditions from a measurement of $u(z)$ at a single height.

The assumptions behind von Kármán's law are discussed by Barenblatt (1996, 2003a), who argues that the assumption of Reynolds-number independence in the limit of large Re is not valid, and that the velocity profile is more

[1] $\overline{u'w'}$ can be measured directly with a fast-responding sonic anemometer, but this is much more expensive than just measuring the mean velocity. Surface stress can be measured directly with a drag plate, which is also expensive, and it is very difficult to get a reliable result (Kaimal & Wyngaard, 1990; Kaimal & Finnigan, 1994, section 6.3).

generally described by a power law:

$$\frac{u(z)}{u_*} = \left(\frac{\sqrt{3}}{2\alpha} + \frac{5}{2}\right)\left(\frac{zu_*}{\nu}\right)^{\alpha} \equiv A(\alpha), \qquad \nu \text{ is kinematic viscosity} \tag{2.3}$$

For flow in a pipe the power α would be equal to $3/(2\ln Re)$, but for flow across a flat plane Re is not uniquely defined, and α must be determined by fitting data to the curve. Barenblatt does not consider surface roughness, which is significant for any natural terrain besides very smooth ice (Sutton, 1953, sec. 3.8, 7.2; Panofsky & Dutton, 1984, sec. 6.2).

Turbulence generated by heat flux. There is usually a significant temperature gradient in the surface layer. During the day, as the sun heats the ground, air near the ground is warmer and less dense than air above, so it is unstable to vertical displacements. In this case buoyant forces promote turbulence, converting gravitational potential energy to turbulent kinetic energy. At night, the temperature gradient is reversed, and turbulence is suppressed. Neutral stability is rare, and is only approached when the sky is heavily overcast, so the ground is not gaining or losing energy by radiation, and in addition there is moderate or high wind so the air is well mixed in temperature.

The velocity profile in thermally stratified turbulent flows is observed to deviate from the logarithmic law. A general description of turbulence with heat flux is provided by the Monin-Obukhov similarity theory (Monin & Yaglom, 1971, chap. 7), in which all dimensionless quantities depend on one dimensionless variable,

$$\zeta = \frac{z}{L}, \quad L \equiv -\frac{{u_*}^3}{\kappa(g/T_0)(q/c_p\rho_0)},$$

u_* : friction velocity
g : gravity
T_0 : mean absolute temperature
q : upward heat flux at surface
c_p : heat capacity
ρ_0 : mean density

The turbulent heat flux is due to covariance of vertical velocity and temperature: $q = c_p\rho_0\overline{w'T'}$, where T' is the fluctuating component of temperature. It can be shown (Monin & Yaglom, 1971) that ζ represents a ratio of buoyant generation of turbulence to mechanical shear generation. Thus, at large heights buoyant forces are relatively more important than at small heights, where the ground suppresses the larger eddies. The theory also assumes $z \gg z_0$, and therefore does not apply within a few meters above large obstacles such as trees and buildings.

By dimensional analysis, the velocity profile has the form

$$\frac{\kappa z}{u_*}\frac{\partial u}{\partial z} = \varphi_m(\zeta), \quad \varphi_m(0) = 1 \tag{2.4}$$

The dimensionless function $\varphi_m(\zeta)$ must be determined by experiment. The observations have been fit to a variety of functions, and the Businger-Dyer formula is a widely used simple approximation (Arya, 1999, sec. 4.7.2):

$$\varphi_m(\zeta) = (1 + 15|\zeta|)^{-1/4}, \qquad -5 < \zeta < 0 \text{ (unstable)}$$
$$\varphi_m(\zeta) = 1 + 5\zeta, \qquad 0 \le \zeta < 1 \text{ (stable)}$$

As before, the profile $u(z)$ can then be obtained by integrating this function from z_0 to z. Similarly, dimensionless functions can be defined for the gradients of temperature[2] and concentration, and these also have been determined empirically.

Since a direct measurement of heat flux requires expensive instruments[3], formulas have been worked out to estimate u_* and L from the mean wind speed and temperature measured at two heights (Arya, 1999, sec. 4.8.1; Arya, 1988, sec. 11.5.6).

Power-law profile as approximate description. If the Monin-Obukhov profile is impractical (for example if it is too complex, if temperature is not available, or if terrain is not uniform), meteorologists and engineers have long resorted to a simple equation (Panofsky & Dutton (1984, sec. 6.3); Sutton (1953, sec. 7.2)),

$$\frac{u}{u_1} = \left(\frac{z}{z_1}\right)^{\alpha}, \tag{2.5}$$

where u_1 and z_1 are a reference velocity and reference height, and α is found by fitting the equation to measurements of u at two or more heights. Although equation (2.5) lacked theoretical justification until the work of Barenblatt (2003a), it provided a reasonable fit to wind profiles in the surface layer over a wide range of surface roughness and stability conditions, and is frequently used in air pollution modeling (Arya, 1999, sec. 4.8.3). Experimentally, the exponent α can range from nearly 0, representing perfect mixing and a uniform velocity profile, to nearly 1, representing the Couette linear profile of laminar motion over a plane surface. Increasing surface roughness and instability promote mixing and correspond to smaller α.

2.2. **Turbulent diffusion.**

The gradient transport assumption. The simplest model of turbulent transport is based on the analogy to molecular diffusion. It is assumed that the mean (that is, time-averaged) flux is linearly proportional to the gradient of mean density:

$$\text{for momentum,} \quad \tau = \rho K_m \frac{\partial u}{\partial z} \quad \text{(positive downward)} \tag{2.6}$$

$$\text{for admixture concentration,} \quad \mathbf{F} = -K_c \boldsymbol{\nabla} c \quad \text{(positive upward)} \tag{2.7}$$

[2]Strictly speaking, this is potential temperature, which is the temperature a parcel of air at height z would have if brought adiabatically to the pressure at the ground. Near the ground, this is a small correction (Sutton, 1953, sec. 1.3).

[3]$\overline{w'T'}$ can be measured directly by eddy covariance, or the heat flux could be determined from the energy budget if the radiation input and heat flux into the soil are measured.

These K's are called turbulent exchange coefficients.[4] They represent mixing by turbulent eddies, and are usually several orders of magnitude larger than the corresponding molecular viscosity or diffusivity.

Unlike their molecular counterparts, turbulent exchange coefficients depend on the particular flow field—rather than molecular properties—and also vary from one region to another of the same flow (Arya, 1999, sec. 4.6.1). Experiments show that they are definitely not uniform in space: if K_c were spatially uniform and the wind speed were also independent of height, mass injected at a steady rate from a point source at the ground would produce a Gaussian plume, whose height grows with the square root of downstream distance x, and ground-level concentration decreases as $1/x$. However, the plume height is observed to grow as some larger power of distance, 0.75 to 1 instead of 0.5 (Panofsky & Dutton, 1984, sec. 10.3), and the ground-level concentration also decreases faster than $1/x$ (Sutton, 1953, p. 277). Therefore the exchange coefficient cannot be constant, but increases with height; this is because in the atmosphere, there are eddies of a wide range of sizes, and at greater heights, larger eddies contribute to mixing. A constant K_c would imply that there is only one length scale of mixing, a molecular length scale, which is not true in turbulence.

It is sometimes assumed (e.g., Barenblatt (2003b)) that the ratio of the K's for momentum and concentration is independent of height:

$$K_c(z) = (\text{constant})K_m(z).$$

This assumption implies that the mechanisms of turbulent transfer for the passive admixture are the same as for momentum. However, observations suggest that this ratio does depend slightly on z/L in unstable conditions, though not in stable conditions. The ratio at neutral stability is generally taken to be 1, although there is disagreement over this value in the literature (Kaimal & Finnigan (1994, sec. 1.3.5); Brown *et al.* (1993, sec. 3c); Panofsky & Dutton (1984, sec. 6.9)).

Implications of constant flux. Fluxes and concentration gradients are expensive to measure directly, and so various assumptions are used to estimate $K(z)$. It is generally believed that the fluxes of momentum, heat, and mass are approximately independent of height within the surface layer. If the assumption of constant flux is valid, then $u_* = \sqrt{\tau/\rho}$ is independent of height. Then (2.6) can be written as

$$K_m(z) = \frac{{u_*}^2}{\partial_z u} \tag{2.8}$$

and using equation (2.4) leads to an expression for $K_m(z)$ (Kaimal & Finnigan (1994); Panofsky & Dutton (1984, sec. 6.8)):

$$K_m(z) = \frac{k u_* z}{\phi_m(\zeta)} \tag{2.9}$$

[4]They are really tensors, but the only significant components are the xz component of K_m and the zz component of K_c.

and analogous expressions for the K's for heat and mass. At neutral stability where $\zeta = 0$ and $\phi_m = 1$, (2.9) predicts

$$K_m(z) = k u_* z. \tag{2.10}$$

If the velocity profile follows the power law (2.5), and if u_* can be treated as constant, then (2.8) predicts

$$K_m(z) = \frac{{u_*}^2}{\partial_z u} = \frac{{u_*}^2 z_1}{u_1 \alpha} \left(\frac{z}{z_1} \right)^{1-\alpha}. \tag{2.11}$$

Equations (2.5) and (2.11) are known in meteorology as "Schmidt's conjugate power laws." However, the assumption of constant flux is not necessarily consistent with the assumption of power law profiles for velocity and diffusivity, so the diffusivity is often modeled instead as

$$K(z) = K_1 \left(\frac{z}{z_1} \right)^m, \tag{2.12}$$

where the parameters could be determined by fitting the power function to (2.9), and usually $m + \alpha > 1$ (Arya, 1999, sec. 4.8.5).

Limitations. The gradient-transport equations (2.6, 2.7) assume that the flux at a point depends only on the local gradient. This assumption fails if the eddies are large compared to the scale of curvature of the profile. If there are eddies large enough to carry air between regions of significantly different gradient, the actual flux can be non-local and even opposite the local gradient (Arya, 1999, sec. 4.6.1; Panofsky & Dutton, 1984, sec. 4.7.2; Pasquill & Smith, 1983, sec. 3.1). Such large eddies occur most often in very unstable conditions, such as on a clear sunny day with light winds, where buoyancy-generated convection is the dominant source of turbulence. Under these conditions "looping" plumes are seen, as the large eddies move the plume as a whole back and forth, instead of the spreading or "coning" plumes predicted by gradient-transport theory (Arya, 1999, sec. 6.8). Thus gradient-transport theory is most valid when mechanical shear is dominant, with slightly unstable, neutral or stable temperature profiles and strong winds.

Slender plume approximation. Turbulent diffusion in the x direction may be neglected when advection dominates dispersion in the far downwind limit, i.e., x large compared to K/u. (Typically K is of the order of 1–10 m^2/s and u of the order of 1–10 m/s, so x should be large compared to 1 meter.) It is also possible, but more cumbersome, to solve the advection-dispersion equation (2.1) including diffusion in the x direction and then take the limit for $x \gg K/u$, which leads to the same result; see, for example, Sutton (1953, sec. 4.6), or Huang (1979). Neglecting such diffusion is called the slender plume approximation (Arya, 1999, sec. 6.3.6). With this approximation, the concentration will be zero everywhere upwind of the source.

3. Analytical and numerical solutions of the advection-dispersion equation

Both solutions of equation (2.1) discussed here make two further simplifying assumptions:

- The flow is stationary and the source remains constant in time for long enough to establish a steady-state concentration field. For the numerical simulation, this assumption was not actually necessary, but was used to provide a simple test case.
- The source is independent of the crosswind direction, y, so the concentration depends only on x and z; that is, the problem is two-dimensional. This assumption is equivalent to considering only the cross-wind integrated concentration,

$$\bar{c}_y \equiv \int_{-\infty}^{\infty} c(\mathbf{x}, t)\, dy.$$

  Meteorologists sometimes use this simplification and then assume a Gaussian distribution in the lateral direction. The lateral diffusivity depends on distance from the source and atmospheric stability, and is often estimated using the empirically derived Pasquill-Gifford diagrams (Arya (1999, sec. 6.6.4); Pasquill & Smith (1983, sec. 3.2)).

With these assumptions, the advection-dispersion equation (2.1) has been reduced to

$$u(z)\partial_x c(x,z) = \partial_z \left(K_c(z)\partial_z c(x,z)\right). \tag{3.1}$$

3.1. **Analytical solution and interpretation.**

Steady Propagation from Line Source. An analytical solution to (3.1) is known when the velocity and diffusivity are given by power laws, and the additive is injected at a constant rate from an infinite straight line on the ground perpendicular to the wind. In other words, end effects are neglected; hence the solution will overestimate the concentration from any finite source. The problem is now

$$\begin{aligned} &u(z)\partial_x c(x,z) = \partial_z \left(K_c(z)\partial_z c(x,z)\right), \text{ for } x > 0 \text{ and } z > 0, \text{ with} \\ &u(z) = u_1 \left(\frac{z}{z_1}\right)^{\alpha}, \\ &K_c(z) = K_1 \left(\frac{z}{z_1}\right)^{m}. \end{aligned} \tag{3.2}$$

Solutions are known for boundary conditions specifying concentration at the ground, flux at the ground, or a linear combination of the two (Philip, 1959). The flux-type boundary condition will be discussed here. Two boundary conditions are implied by the physical model. First, no flux crosses the ground for $x > 0$:

$$K_c(z)\partial_z c \to 0 \text{ as } z \to 0 \tag{3.3}$$

(If the admixture is absorbed or interacts with the ground, this is not valid.) Second, there is a known constant source. Integrating (3.2) from $z = 0$ to ∞ gives

$$\partial_x \int_0^\infty u(z)c(x,z)dz = K_c(z)\partial_z c\big|_0^\infty = 0, \text{ so}$$

$$\int_0^\infty u(z)c(x,z)dz = Q, \text{ a constant independent of } x. \tag{3.4}$$

Q is the rate of injection by the source at the origin. Since there is no absorption, in the steady state the total flux of admixture across any vertical line at $x > 0$ is equal to the rate of injection.

Solution and interpretation. Equation (3.2) can be solved by the method of similarity, which applies when a function of two variables has a symmetry so that it actually depends only on a single, dimensionless combination of the two variables.

The solution for the concentration can be presented as the product of a ground-level concentration $c_{gl}(x)$ and a plume height function $c_{ph}(x,z)$:

$$\begin{aligned} &c(x,z) = c_{gl}(x)c_{ph}(x,z), \text{ where} \\ &c_{gl}(x) = \frac{Q}{u_1 z_1}\frac{r}{\Gamma(\beta)}\left(\frac{x}{x_1}\right)^{-\beta}, \\ &c_{ph}(x,z) = \exp\left\{-\frac{(z/z_1)^r}{x/x_1}\right\}, \\ &r = 2 - m + \alpha, \quad \beta = \frac{1+\alpha}{r}, \quad x_1 = \frac{u_1 {z_1}^2}{r^2 K_1}. \end{aligned} \tag{3.5}$$

Equation (3.5) has appeared many times in the literature (Deacon, 1949; Calder, 1949; Sutton, 1953; Monin & Yaglom, 1971; Huang, 1979; Pasquill & Smith, 1983; Panofsky & Dutton, 1984; Arya, 1999). Barenblatt (2003b) explains how the solution is obtained.

Figure 3.1 shows contours of $c(x,z)$. The first plot has $\alpha = 1/7$, typical for neutral stability. The second has $\alpha = 0.3149$ chosen to fit the logarithmic velocity profile in the simulation, as seen below in Figure 4.1. The larger α leads to less mixing and less upward transport.

According to (3.5), the plume height grows as $x^{1/r}$, and the ground-level concentration decreases as $x^{-\beta}$. The concentration is inversely proportional to the wind speed u_1, as usual for advection. Some important limiting cases are:

- For uniform wind ($\alpha = 0$) and uniform diffusivity ($m = 0$), (3.5) reduces to a Gaussian vertical profile:

  $$c(x,z) = \frac{Q/u_1}{\sqrt{\pi K_1 x/u_1}} \exp\left(-\frac{z^2}{4K_1 x/u_1}\right)$$

  However, this equation is not a good fit to observed profiles in field and wind tunnel experiments (Brown *et al.* , 1993).

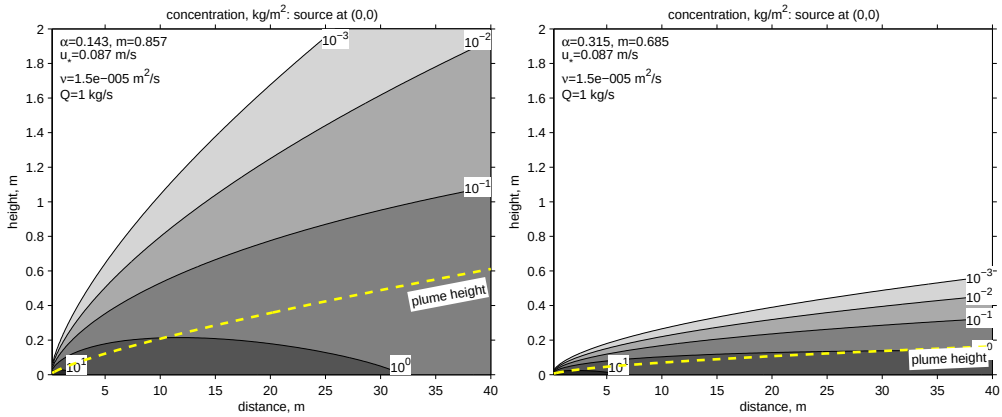

Figure 3.1: Contours of plume (3.5) for two values of α, representing different amounts of mixing: larger α means less mixing. The dashed line shows the height where $c(x, z)$ is $1/e$ of its value at the ground: $z_h = z_1(x/x_1)^{1/r}$. The value of u_* is the one used in Oldenburg & Unger (2004) for the wind speed of 1 m/s at a height of 10 m.

- If the conjugate power laws (2.5, 2.11) hold, then $m = 1-\alpha$, $r = 1+2\alpha$. For $\alpha = \frac{1}{7}$, a typical value for neutral stability, this gives $\beta = \frac{8}{9}$; Sutton (1953, p. 281) cites observations of the propagation of smoke from a line source over level downland in neutral conditions, where the ground-level concentration was observed to decrease as $x^{-0.9}$, corresponding to $\beta = 0.9$.

This solution is the response of the system to mass injected at the line $(x, z) = (0, 0)$. If instead the source is spread over the ground with a density of $S(x)$, the solution is the convolution

$$c(x,z) = \int_{-\infty}^{x} S(x')\, c_{\text{line}}(x-x', z)\, dx' \tag{3.6}$$

where $c_{\text{line}}(x, z)$ is the solution for a unit line source:

$$\begin{aligned} c_{\text{line}}(x,z) &= \frac{1}{u_1 z_1}\frac{r}{\Gamma(\beta)}\left(\frac{x}{x_1}\right)^{-\beta} \exp\left\{-\frac{(z/z_1)^r}{x/x_1}\right\}, \quad x > 0; \\ &= 0, \quad x \le 0. \end{aligned}$$

3.2. **Coupled simulation of air and subsurface transport.** Oldenburg & Unger (2004) used the integral finite difference code TOUGH2 (Pruess *et al.* , 1999; Pruess, 2004) to simulate the transport of CO_2 leaking from a geologic sequestration site. The CO_2 mixes with soil gas and also dissolves in groundwater, eventually seeping out of the ground. The authors evaluated whether it would reach hazardous concentrations above ground. The wind velocity profile was logarithmic:

$$u = \frac{u_*}{k} \ln \frac{z}{z_0} \tag{3.7}$$

with u_* chosen to give a desired value of u at a reference height of $z = 10$ m, $u = 1$ m/s or $u = 5$ m/s representing typical slow and fast wind speeds; $k = 0.4$; and $z_0 = 0.10$ m. TOUGH2 cannot specify the wind velocity profile directly; instead, a horizontal pressure gradient was imposed, and an artificial height-dependent "permeability" was specified in the cells above ground such that Darcy's law would yield the desired horizontal flow speed. The resulting horizontal wind speed was not quite independent of x, and the vertical wind speed of gas above ground was not exactly zero, perhaps due to discretization and round-off errors.

The vertical diffusivity above ground was given using the constant flux assumption (2.10):

$$K = ku_*z.$$

The integral finite difference method produces numerical dispersion in the horizontal direction on the order of one-half the grid spacing multiplied by the horizontal wind velocity. To prevent the plume from unrealistically spreading upwind, the vertical diffusivity K was set to zero upwind of the source.

Figure 3.2 shows the computed mass fraction of CO_2 in air at a quasi-steady state (6 months after injection begins in the simulation). Figure 3.3 shows the same data zoomed in on an area above the ground and directly above the area where CO_2 was injected. These figures show selected contour lines interpolated from the grid.

A very small fraction of CO_2 has diffused from the air back into the ground downwind of the plume, and is slowly diffusing deeper; it also dissolves in groundwater which is moving downward.

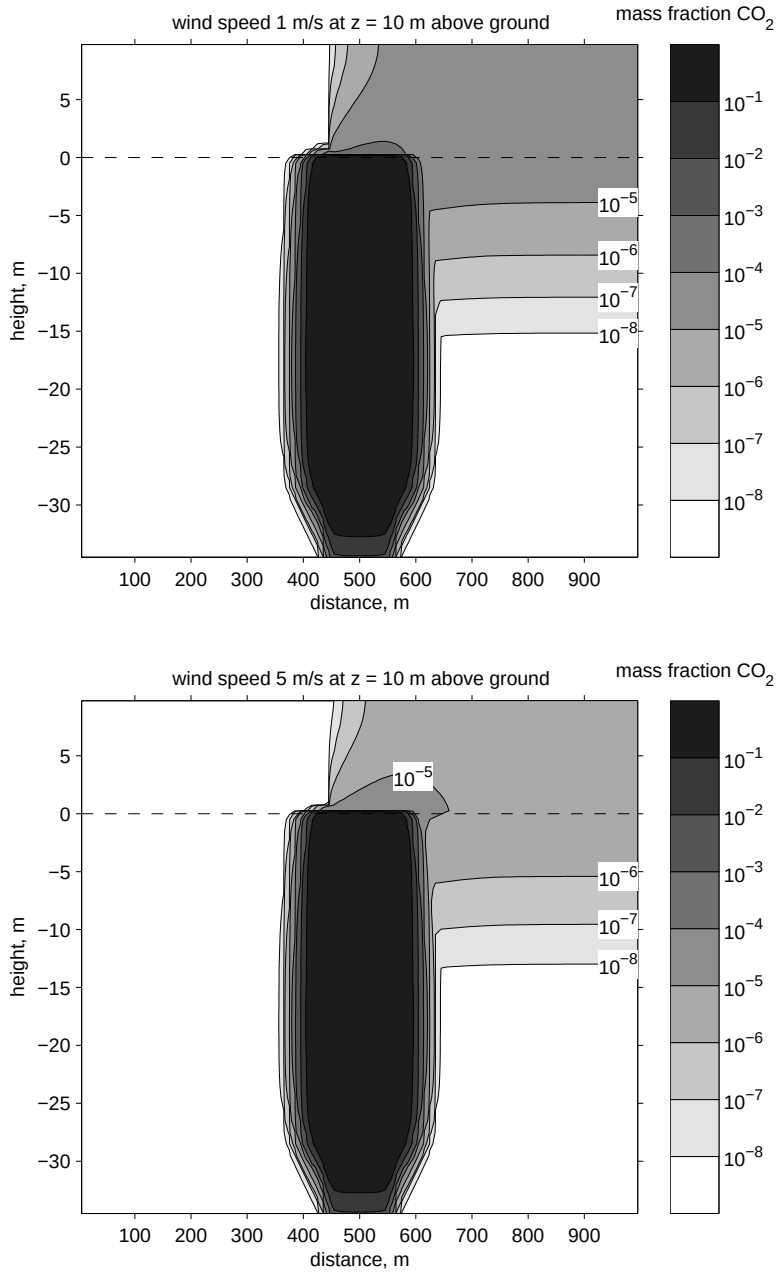

Figure 3.2: Mass fraction CO_2 in gas for slow and fast wind speeds. Similar to Figure 9ab in Oldenburg & Unger (2004); redrawn from data kindly provided by the authors. CO_2 is driven upward by high pressure at the source, displacing soil gas in the subsurface plume. In the second figure it can be seen that the concentration in the subsurface, where the time scale of propagation is slower, has not yet reached equilibrium with the air downwind of the source: see the 10^{-5} contour.

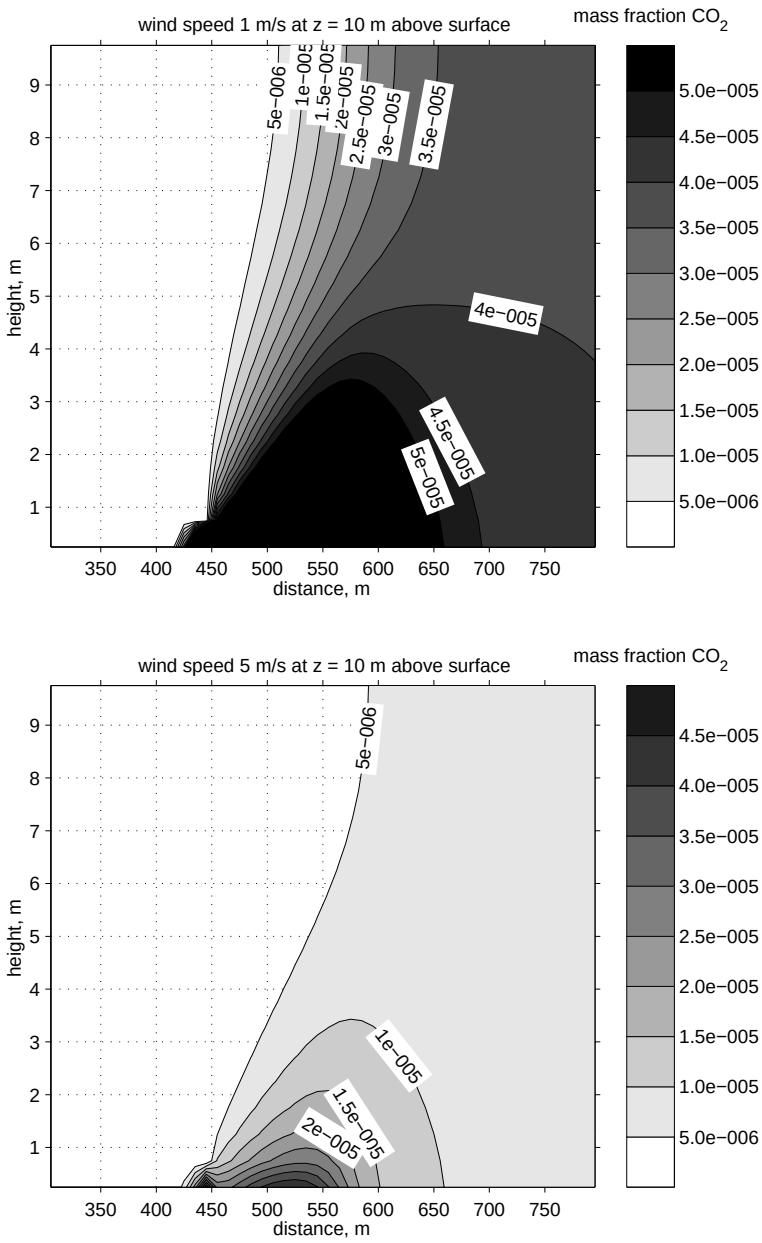

Figure 3.3: Mass fraction CO_2 in gas for slow and fast wind speeds. Same data as previous figure, showing a smaller region with different contour levels. As usual for advection, the concentration is inversely proportional to wind speed (5 times smaller for the 5 times faster wind speed). Note that contour lines are perpendicular to the top surface, which is an artifact of using a closed top boundary condition. Also, the spike at $x = 450$ m is caused by the artificial suppression of vertical dispersion upwind of the source.

4. Comparison and conclusions

4.1. **Comparison of two solutions.** To compare this simulation with the analytic solution, the logarithmic profile was approximated by a power law. Figure 4.1 shows the velocity at the grid points of the simulation, with fits to $u = u_1 z^\alpha$ by Matlab's curve fitting tool; one fit is unweighted and the other is weighted by the difference between successive values of u. There is no unique criterion to choose the most appropriate fit.

The unweighted fit was used for the velocity profile. The diffusivity was derived from the conjugate power law (2.11), resulting in generally smaller K (Figure 4.2) and reducing the upward transport of the admixture compared to the simulation.

In the simulation, CO_2 passes from the ground to the air over an extended area. Therefore, it should be compared with the analytical solution using equation (3.6). Since the flux of CO_2 across the ground surface was not

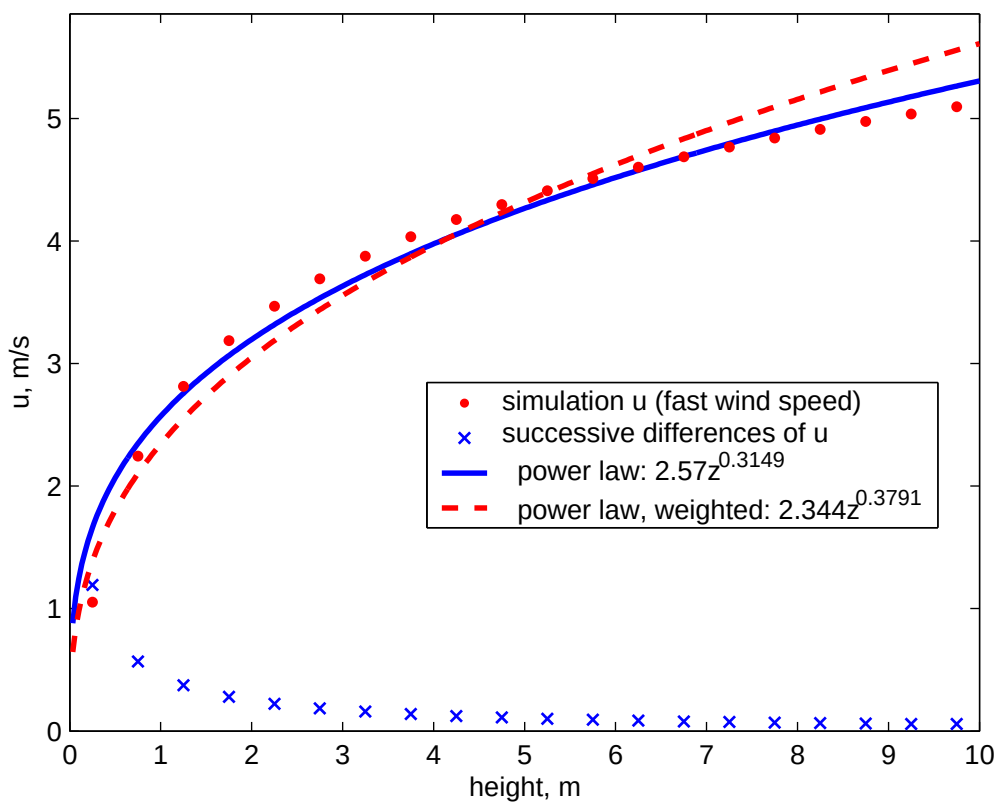

Figure 4.1: Horizontal wind speed in the simulation, and power-law fits.

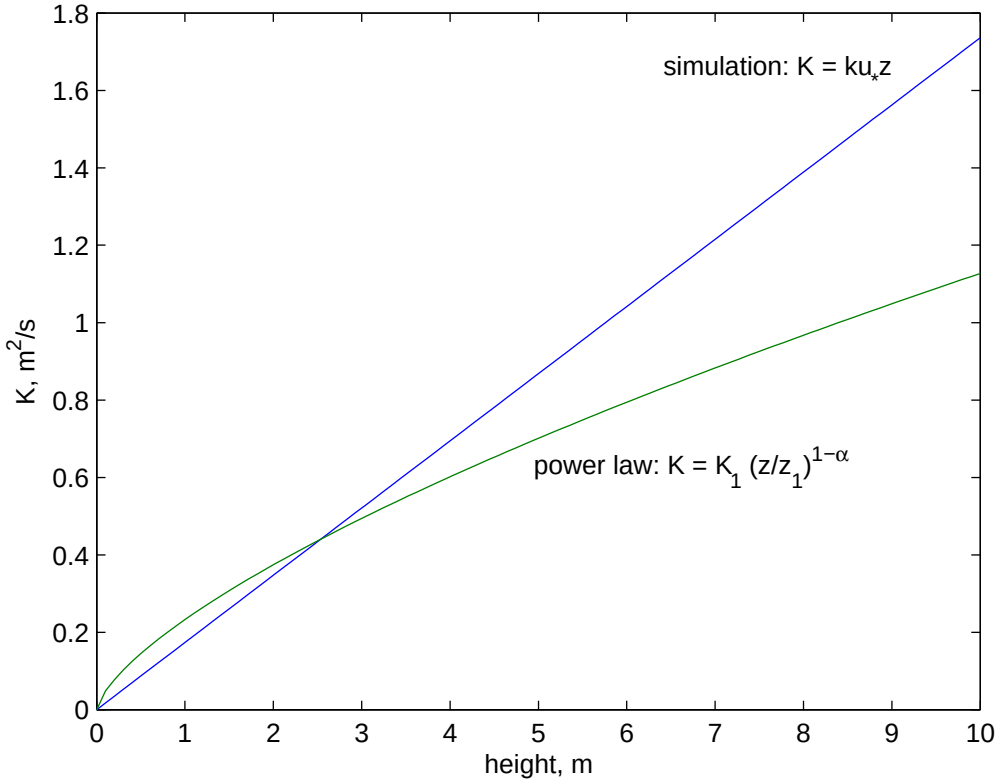

Figure 4.2: Vertical diffusivity from equation (2.10) for the logarithmic profile and equation (2.11) for the power-law profile in Figure 4.1.

directly available, the source density was inferred by

$$S(x) = \frac{d}{dx}\int_0^\infty X^{\mathrm{CO}_2}(x,z)F_{gx}(x,z)\ dz,$$

$$X^{\mathrm{CO}_2} = \text{mass fraction } \mathrm{CO}_2 \text{ in gas}, \quad F_{gx} = \text{horizontal flux of gas}$$

which is shown in Figure 4.3. The reverse seepage flux of CO_2 back into the ground can also be calculated, since the horizontal flux declines very slightly downwind of its maximum at about $x = 600$ m; the loss is about 10^{-5} of the maximum flux. The source density for the other data set (wind speed 1 m/s) was indistinguishable, because the seepage of CO_2 was driven by a high pressure at 30 m below the surface, and did not depend on the wind speed above the ground.

Figure 4.4 shows the result of the convolution and compares it with the simulation. It is qualitatively similar to the TOUGH2 plume, but does not show the artifacts of the closed top boundary condition and the suppression of upwind diffusion. Figure 4.5 compares the concentrations at $z = 0.75$, near the ground, and at $z = 9.75$, the top of the simulation. The simulation reaches a larger

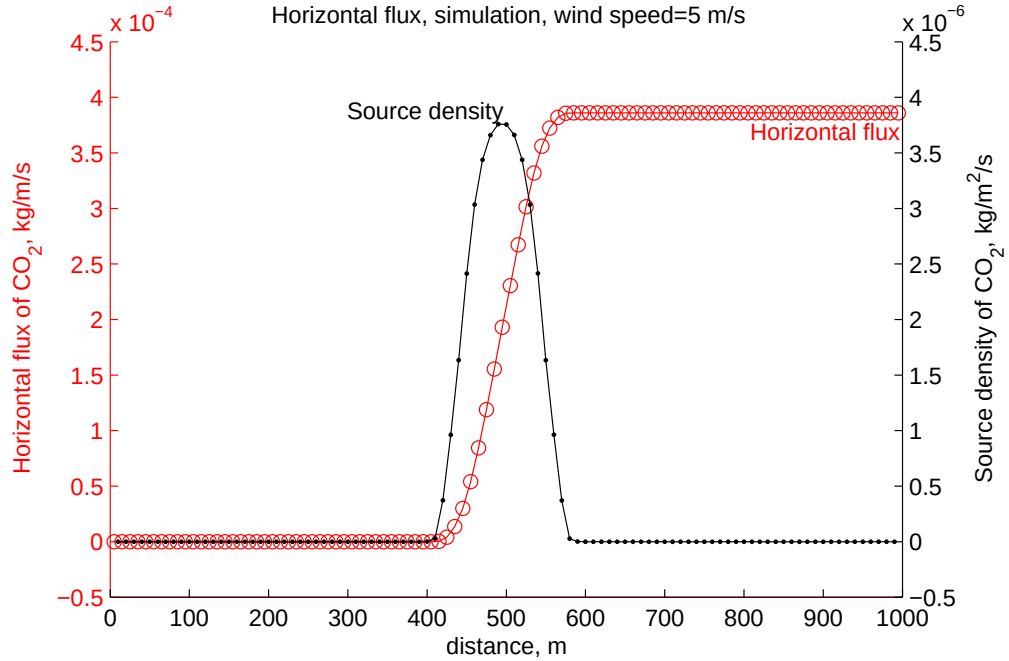

Figure 4.3: Source density of CO_2 from ground to air calculated from simulation result. The circles indicate total horizontal flux at gridpoints x_i calculated by $f_i = \sum_{z_j>0} X^{CO_2}(x_i, z_j) F_{gx}(x_i, z_j)\,\Delta z$. The source density is then calculated from the successive differences, $S_{i+0.5} = (f(x_{i+1}) - f(x_i))/\Delta x$. A linear interpolation of this source density is used in the convolution (3.6). The horizontal flux declines very slightly downwind of its maximum, due to reverse seepage of CO_2 back into the ground; the loss is about 10^{-5} of the maximum flux, too small to see on the graph.

maximum and decays more slowly with downwind distance, likely because of the boundary conditions.

The aboveground domain has much shorter inherent time scales than the underground domain. In the simulation, the permeability changes abruptly from 1 darcy just below the ground to 2×10^9 darcy just above, and from horizontal gas speeds of the order of 10^{-7} m/s below to 1 m/s above. It is difficult for the code to maintain accurate calculations at such a boundary. Figure 4.6 illustrates how the smooth distribution of vertical gas velocities under the surface suddenly becomes irregular and noisy in the air.

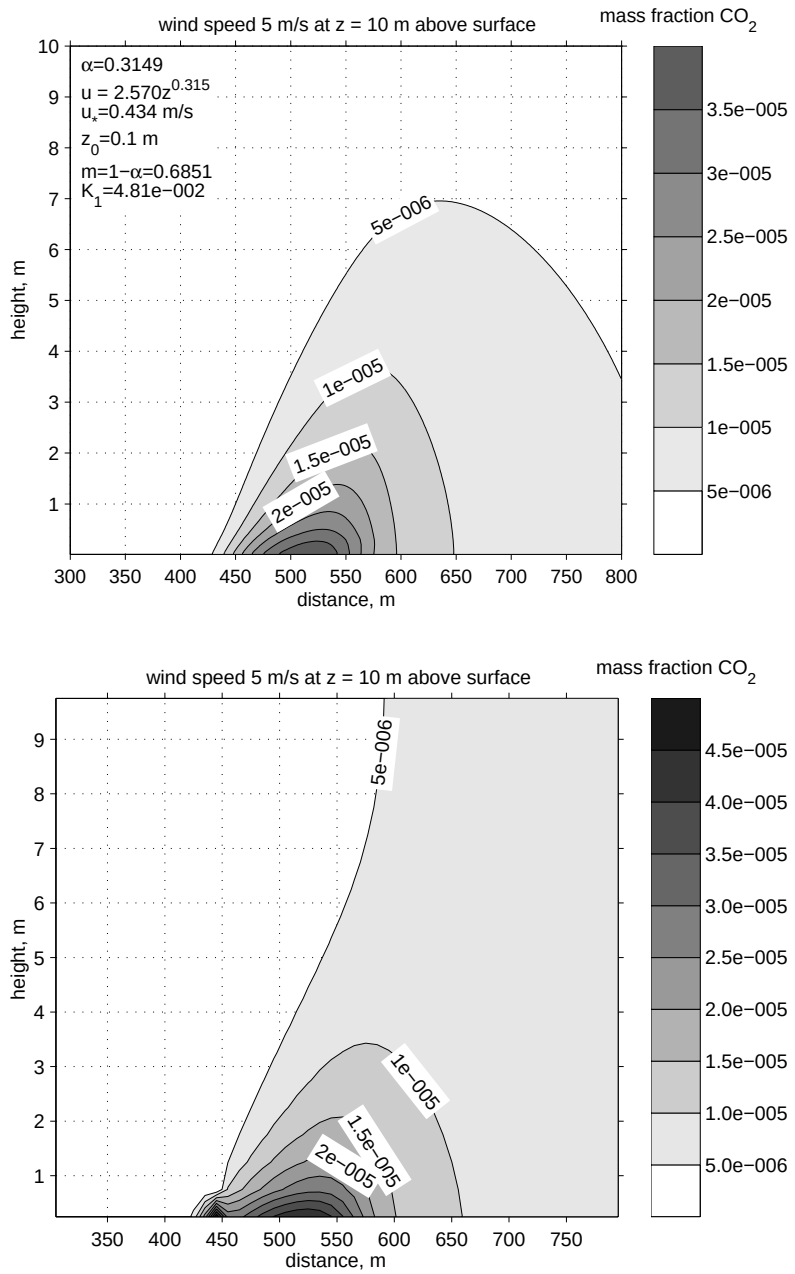

Figure 4.4: Convolution of line-source kernel for fast wind speeds with source distribution from Figure 4.3 (top). Compare to coupled simulation (bottom). Contours near the ground are similar, but there is less upward transport with the power-law velocity and diffusivity functions. The analytical solution does not have the closed top boundary condition and the artificial barrier to upwind diffusion. The concentration fields for the slower wind speed are similar but 5 times larger because of the factor of $1/u_1$.

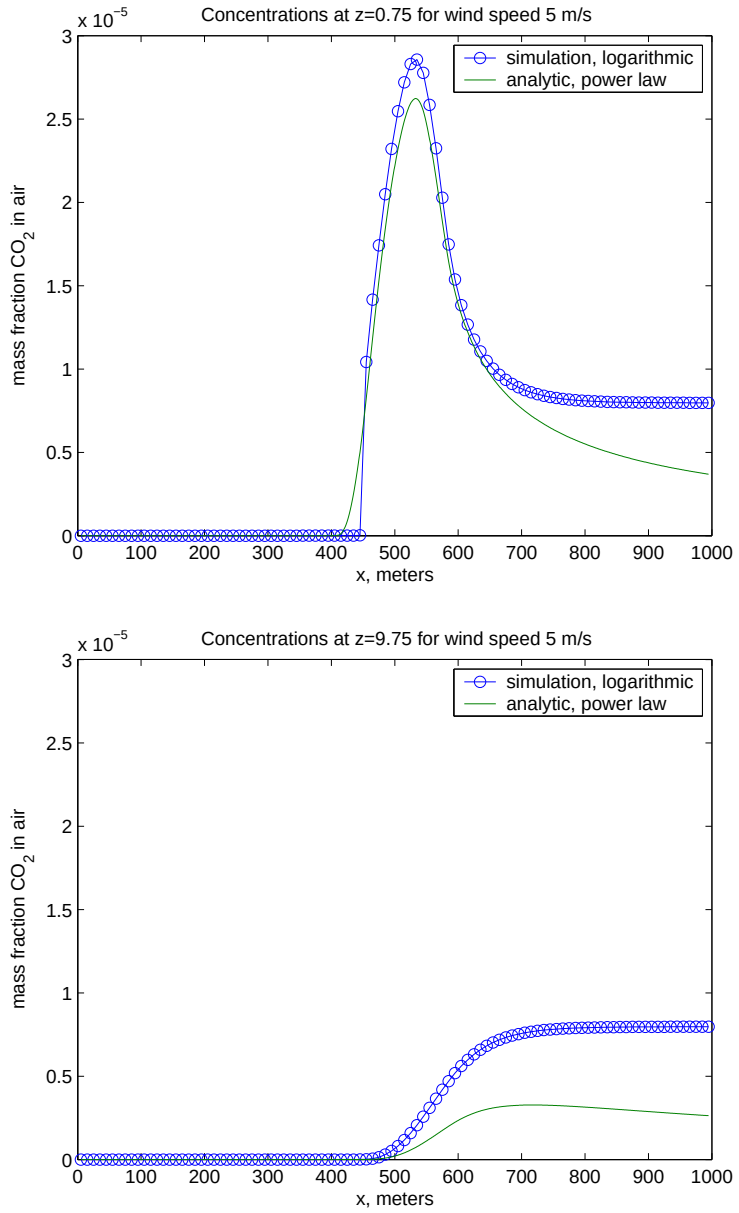

Figure 4.5: The two solution methods compared at heights of $z = 0.75$ m and $z = 9.75$ m. The simulation reaches a larger maximum and decays more slowly with downwind distance, possibly because of the closed top boundary condition. Also, a zero-gradient side boundary condition was imposed on the simulation (i.e., $\partial c/\partial x = 0$ at $x = 1000$), which causes the concentration to reach a constant value at relatively small downwind distances, instead of decaying to zero only asymptotically as $x \to \infty$. Both these boundary conditions would lead to accumulating CO_2 in the simulation, rather than letting it escape to infinity in the vertical and horizontal.

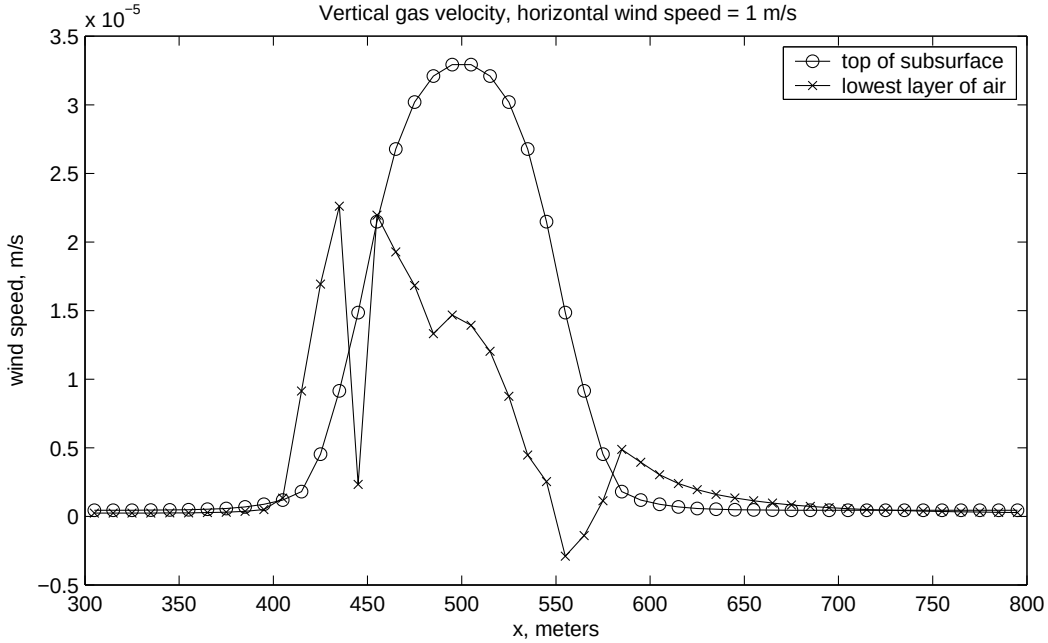

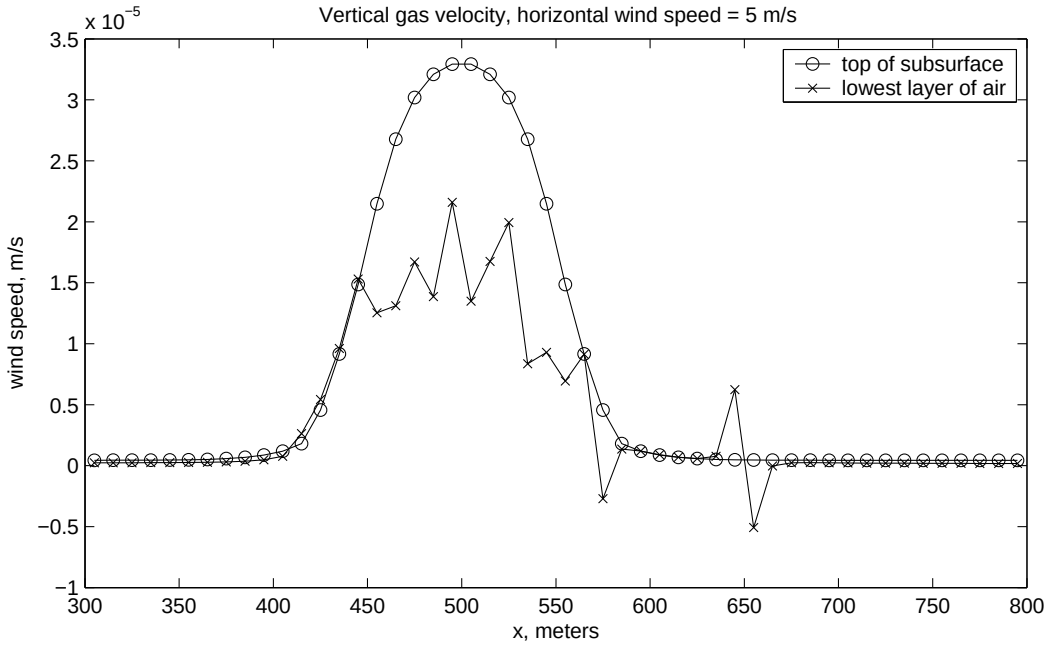

Figure 4.6: Vertical gas velocity in the simulation at the top layer of the subsurface and the bottom layer of air.

4.2. **Conclusions.** Both approaches described here are limited by the highly simplified model of turbulent diffusion. The gradient-transport model assumes that flux of momentum and mass is constant with height, transport is local, and the exchange coefficients for mass and momentum differ only by a constant factor, as described in section 2. The model applies only to heights above any surface obstacles and large compared to z_0; it assumes flat ground with short, homogeneous vegetation. Modeling the roughness sublayer, which is significant above trees or buildings, would be far more complex.

The TOUGH2 coupled simulation is intended to model barometric pumping and reverse seepage of air contaminants back into the ground under conditions where it could be significant, such as with large soil permeabilities. But the underground and aboveground domains operate on vastly different time and space scales, raising a question of whether a single numerical model can handle both. This question could be avoided by separating the domains whenever they are not strongly coupled. We expect on *physical* grounds that the air above ground is not usually coupled to the subsurface, because the capillary entry pressure for gas into the ground is high enough that the ground can be treated as a reflecting boundary. In fact, this was a good approximation in the case used for the simulation, as shown by getting the same emission rate out of the ground for both wind speeds. If the main goal is to predict concentrations in the air, the small reverse seepage (only 10^{-5} as great as the total flux of CO_2 into the air) could be neglected.

Each approach has advantages and disadvantages. Some advantages of the analytical solution, as opposed to the coupled simulation, are:

- It is computationally simple and needs no programming, while still taking into account the variation of K with height.
- It does not suffer from the closed-top boundary condition imposed by TOUGH2 (although TOUGH2 could work around this limitation by adding a very large grid block above the layer of interest to receive the upward flux).
- It does not have the artificial horizontal dispersion which accompanies advection in the numerical solution.
- There is no minimum grid cell size. TOUGH2 cannot make the grid cell smaller than the roughness length, z_0, while using the logarithmic velocity profile.
- There are no problems of finite precision.

Disadvantages of the analytical solution:

- The solution is known only for power-law profiles. It is questionable how accurately a logarithmic or Monin-Obukhov profile can be approximated by a power law. In particular, the diffusivity will always grow more slowly at large heights for power laws than for the logarithmic profile. Therefore, the analytic solution predicts less transport of the admixture upward, as seen in Figure 4.4.

- It cannot describe a time-dependent source profile, which could easily be handled in TOUGH2.
- It cannot describe a three-dimensional problem in general.
- The slender plume approximation fails for wind speeds approaching zero, which is also the worst condition for building up high local concentrations of contaminants.

These shortcomings could be addressed by using a numerical simulation of the air; many off-the-shelf products are available (New Zealand Ministry for the Environment, 2004).

Acknowledgments. We are grateful to Dr. Oldenburg of Lawrence Berkeley National Laboratory, Earth Sciences Division, for sharing his data, helping us interpret it, and carefully reviewing this report. The authors would also like to thank Professor G. I. Barenblatt, who read an early version of the report and provided very useful discussions.

This work has been performed at University of California, Berkeley, and Lawrence Berkeley National Laboratory of the U.S. Department of Energy under Contract No. DE-AC02-05CH11231. Support for the first author was provided by a Sunset Fellowship from the Center for Pure and Applied Mathematics at UC Berkeley.

References

Arya, S. Pal. 1988. *Introduction to Micrometeorology.* Academic Press.

Arya, S. Pal. 1999. *Air Pollution Meteorology and Dispersion.* Oxford University Press.

Barenblatt, G. I. 1996. *Scaling, Self-similarity, and Intermediate Asymptotics.* Cambridge University Press.

Barenblatt, G. I. 2003a. *Scaling.* Cambridge University Press.

Barenblatt, G. I. 2003b. Transfer of a Passive Additive in a Turbulent Boundary Layer at Very Large Reynolds Numbers. *Proceedings of the National Academy of Sciences, USA*, **100**, 1481–1483.

Brown, Michael J., Arya, S. Pal, & Snyder, William H. 1993. Vertical Dispersion from Surface and Elevated Releases: An Investigation of a Non-Gaussian Plume Model. *Journal of Applied Meteorology*, **32**, 490–505.

Calder, K. L. 1949. Eddy Diffusion and Evaporation in Flow over Aerodynamically Smooth and Rough Surfaces: A Treatment Based on Laboratory Laws of Turbulent Flow with Special Reference to Conditions in the Lower Atmosphere. *Quarterly Journal of Mechanics and Applied Mathematics*, **2**, 153–176.

Deacon, E. L. 1949. Vertical Diffusion in the Lowest Layers of the Atmosphere. *Quarterly Journal of the Royal Meteorological Society*, **75**, 89–103.

Huang, C. H. 1979. A Theory of Dispersion in Turbulent Shear Flow. *Atmospheric Environment*, **13**, 453–463.

Kaimal, J. C., & Finnigan, J. J. 1994. *Atmospheric Boundary Layer Flows: Their Structure and Measurement.* Oxford University Press.

Kaimal, J. C., & Wyngaard, J. C. 1990. The Kansas and Minnesota experiments. *Boundary-Layer Meteorology*, **50**, 31–47.

Monin, A. S., & Yaglom, A. M. 1971. *Statistical Fluid Mechanics: Mechanics of Turbulence*. MIT Press. English edition updated, augmented and revised by the authors.

New Zealand Ministry for the Environment. 2004 (June). *Good Practice Guide for Atmospheric Dispersion Modeling*. Tech. rept. ME522. New Zealand Ministry for the Environment. Available from `http://www.mfe.govt.nz/publications/air/`.

Oldenburg, C. M., & Unger, A. J. 2004. Coupled Vadose Zone and Atmospheric Surface-Layer Transport of Carbon Dioxide from Geologic Carbon Sequestration Sites. *Vadose Zone Journal*, **3**, 848–857.

Panofsky, H. A., & Dutton, J. A. 1984. *Atmospheric Turbulence: Models and Methods for Engineering Applications*. Wiley.

Pasquill, F., & Smith, F. B. 1983. *Atmospheric Diffusion*. 3rd edn. Ellis Horwood.

Philip, J. R. 1959. The Theory of Local Advection. I. *Journal of Meteorology*, **16**, 535–547.

Pruess, K. 2004. The TOUGH codes - A family of simulation tools for multiphase flow and transport processes in permeable media. *Vadose Zone Journal*, **3**, 738–746.

Pruess, K., Oldenburg, C., & Moridis, G. 1999. *TOUGH2 User's Guide*. Version 2.0 Rep. LBNL-43134 edn. Lawrence Berkeley National Laboratory, Berkeley, CA.

Sutton, O. G. 1953. *Micrometeorology*. McGraw-Hill.

Department of Physics, University of California, Berkeley
E-mail address: `kts@calmail.berkeley.edu`

University of California, Berkeley, 425 Davis Hall, Berkeley, CA 94720, USA; and Lawrence Berkeley National Laboratory, 1 Cyclotron Road, MS 90-1116, Berkeley, CA 94720, USA
E-mail address: `patzek@patzek.berkeley.edu`

Lawrence Berkeley National Laboratory, 1 Cyclotron Road, MS 90-1116, Berkeley, CA 94720, USA; and University of California, Berkeley, 415 Davis Hall, Berkeley, CA 94720, USA
E-mail address: `DSilin@lbl.gov`